

Research Article

Cite this article: Olavarria, J.F., Qi, H., Takahata, T & Kaas, J.H. (2022). Overall patterns of eye-specific retino-geniculo-cortical projections to layers III, IV, and VI in primary visual cortex of the greater galago (*Otolemur crassicaudatus*), and correlation with cytochrome oxidase blobs. *Visual Neuroscience* 39:E007
<https://doi.org/10.1017/S0952523822000062>

Received: 08 May 2022

Revised: 17 August 2022

Accepted: 18 August 2022

Keywords:

galago; greater galago; parallel pathways; ocular dominance columns; columnar organization; CO blobs

Corresponding author: Jaime F. Olavarria,
email: jaime@uw.edu

This paper is dedicated to the memory of Dr. Vivien Casagrande.

The online version of this article is published within an Open Access environment subject to the conditions of the Creative Commons Attribution-NonCommercial-ShareAlike license. The written permission of Cambridge University Press must be obtained for commercial re-use.

© The Author(s), 2022. Published by Cambridge University Press. This is an Open Access article, distributed under the terms of the Creative Commons Attribution licence (<http://creativecommons.org/licenses/by/4.0>), which permits unrestricted re-use, distribution and reproduction, provided the original article is properly cited.

Overall patterns of eye-specific retino-geniculo-cortical projections to layers III, IV, and VI in primary visual cortex of the greater galago (*Otolemur crassicaudatus*), and correlation with cytochrome oxidase blobs

Jaime F. Olavarria¹ , Huixin Qi², Toru Takahata^{3,4} and Jon H. Kaas²

¹Department of Psychology, University of Washington, Seattle, Washington, ²Departments of Psychology and Cell Biology, Vanderbilt University, Nashville, Tennessee, ³Interdisciplinary Institute of Neuroscience and Technology, Zhejiang University School of Medicine, Hangzhou, China, and ⁴Department of Neurology of the Second Affiliated Hospital, Zhejiang University School of Medicine, Hangzhou, China

Abstract

Studies in the greater galago have not provided a comprehensive description of the organization of eye-specific retino-geniculate-cortical projections to the recipient layers in V1. Here we demonstrate the overall patterns of ocular dominance domains in layers III, IV, and VI revealed following a monocular injection of the transneuronal tracer wheat germ agglutinin conjugated with horseradish peroxidase (WGA-HRP). We also correlate these patterns with the array of cytochrome oxidase (CO) blobs in tangential sections through the unfolded and flattened cortex. In layer IV, we observed for the first time that eye-specific domains form an interconnected pattern of bands 200–250 μm wide arranged such that they do not show orientation bias and do not meet the V1 border at right angles, as is the case in macaques. We also observed distinct WGA-HRP labeled patches in layers III and VI. The patches in layer III, likely corresponding to patches of K lateral geniculate nucleus (LGN) input, align with layer IV ocular dominance columns (ODCs) of the same eye dominance and overlap partially with virtually all CO blobs in both hemispheres, implying that CO blobs receive K LGN input from both eyes. We further found that CO blobs straddle the border between layer IV ODCs, such that the distribution of CO staining is approximately equal over ipsilateral and contralateral ODCs. These results, together with studies showing that a high percentage of cells in CO blobs are monocular, suggest that CO blobs consist of ipsilateral and contralateral subregions that are in register with underlying layer IV ODCs of the same eye dominance. In macaques and humans, CO blobs are centered on ODCs in layer IV. Our finding that CO blobs in galago straddle the border of neighboring layer IV ODCs suggests that this novel feature may represent an alternative way by which visual information is processed by eye-specific modular architecture in mammalian V1.

Introduction

The nocturnal greater galagos (*Otolemur crassicaudatus*) are Strepsirrhini primates, belonging to a group that branched early in mammalian evolution from haplorrhini (tarsiers, monkeys, and anthropoids). In greater galagos (bush babies), as in other primates, retinal input is relayed to the lateral geniculate nucleus (LGN) and primary visual cortex (V1) along three major parallel pathways named after the distinct class of retinal ganglion cells from which they originate. These pathways are the magnocellular (M), parvocellular (P), and koniocellular (K) pathways (reviewed in Casagrande & Kaas, 1994). Studies of the projections of these three pathways in greater galago V1 revealed that projections of LGN M and P cells terminate with the upper and lower divisions of layer IV, respectively, with a minor projection to layer VI, whereas K LGN cells project to layers III and I (Lachica & Casagrande, 1992; reviewed in Casagrande & Kaas, 1994).

Previous anatomical studies in greater and lesser galago species provided preliminary evidence of periodicity in layer IV (Glendenning et al., 1976, greater and lesser galago; Casagrande & DeBruyn, 1982, lesser galago; Diamond et al., 1985, lesser galago), and physiological studies suggested the existence of ocular dominance columns (ODCs) in greater galago based on the observation that cells with similar ocular dominance responses were grouped together (DeBruyn et al., 1993). More recently, an optical imaging study in galago revealed clusters of monocular responses (Xu et al., 2005), but because the imaging method used does not

discern patterns of activity from separate layers across the depth of the cortex, the results do not inform about the patterns of LGN projections to specific layers.

It is well established that K LGN cells project in a patchy fashion to layer III in both greater and lesser galago V1 (Casagrande & DeBruyn, 1982; Diamond et al., 1985; Lachica & Casagrande, 1992), but at present it is not known whether the overall patterns of LGN projections to layers IV and VI form separated patches as in layer III, or stripe-like patterns resembling the patterns of ODCs in the macaque monkey (Tootell et al., 1988; Florence & Kaas, 1992; Horton & Hocking, 1996b; Olavarria & Van Essen, 1997) and in some relatively large New World monkeys such as Cebus (capuchin) monkeys (Hess & Edwards, 1987; Rosa et al., 1992) and spider monkeys (Florence et al., 1986), or interconnected bands as in other primate species (Takahata et al., 2014) and cats (Anderson et al., 1988). Similarly, it is not known whether layer III patches are randomly distributed across the expanse of V1, or instead are aligned with layer IV domains of the same eye dominance. This question is of interest given that direct projections to layers III and IV originate from different LGN cell types. Finally, while it has been reported that single axon projections from K LGN cells arborize within cytochrome oxidase (CO) blobs in galago V1 (Lachica & Casagrande, 1992), the relationship between CO blobs and ODCs in galago layer IV has not been examined with anatomical methods. Optical imaging studies in galago (Xu et al., 2005), owl monkey (Kaskan et al., 2007), and New World marmoset (Roe et al., 2005) found no clear relationship between ocular dominance domains and CO blobs, whereas studies in macaque monkey have established that CO blobs are consistently centered on ODCs (Horton, 1984; Blasdel & Salama, 1986; Tootell et al., 1988; Bartfeld & Grinvald, 1992; Yoshioka et al., 1996). Here we address these standing questions in greater galago with the ultimate goal of advancing our understanding of the organization and evolution of the visual system in primates, including humans. To this end, we injected the transneuronal tracer wheat germ agglutinin conjugated with horseradish peroxidase (WGA-HRP) into one eye and examined and correlated the patterns of WGA-HRP and CO labeling in tangential histological sections through the unfolded and flattened cortex.

In layer III, we observed that the WGA-HRP labeling appears as an array of distinct patches that most likely represent the patchy K input to layer III shown previously in galago (Lachica & Casagrande, 1992) and owl monkey (Ding & Casagrande, 1997). In layer VI, we observed distinct patches that appear somewhat larger than the patches in layer III, but of similar density. In granular layers, the labeling adopts the form of interconnected bands or stripes whose overall array is reminiscent of the pattern of ODCs in other primates (e.g., owl monkey [Takahata et al., 2014] and in cats (Anderson et al., 1988). Moreover, we found that the patches in layer III are aligned with ODCs in layer IV of the same eye dominance, and that virtually *all* CO blobs overlap with WGA-HRP labeled patches in layers III. Since only one eye was injected with WGA-HRP, these data imply that all CO blobs receive K LGN input from both eyes, and suggest that these inputs remain largely segregated within CO blobs, consistent with previous studies in galago indicating that a high percentage of cells recorded within CO blobs are monocular (DeBruyn et al., 1993). Moreover, we found that CO blobs typically span the borders between neighboring columns, and sample left and right eye columns in non-biased fashion. Based on these findings, we propose a novel model in which CO blobs straddle the border between neighboring ipsilateral and contralateral ODCs in layer IV, such that the resulting CO

subregions receive largely segregated K LGN input of the same eye dominance as the underlying ODCs.

Materials and methods

Animals

The data on the patterns of ocular domains and CO blobs in the present study come from a total of seven hemispheres from four adult greater galagos (*O. crassicaudatus*) weighing 800–1300 g. All procedures were performed in the Psychology Department of Vanderbilt University, following protocols approved by the Animal Care and Use Committee at Vanderbilt University. The research was conducted in accordance with the animal care guidelines of the National Institutes of Health.

Intravitreal injections

Galagos received monocular intravitreal injections containing 1.5 mg of WGA-HRP (Sigma-Aldrich, St Louis, MO) dissolved in 20 μ L of normal saline. The tracer was delivered during 15–20 min through glass micropipettes driven to about 5–6 mm deep into the posterior chamber of one eye. Anesthesia was induced with Ketaset (0.05 mg/kg, im) and maintained with isoflurane 2%. Arterial pulse oxygenation, pulse rate, respiration rate, and core body temperature were monitored throughout the surgical procedures.

Tissue processing

After a survival period of 4–5 days, the animals were deeply anesthetized with pentobarbital sodium (100 mg/kg i.p.) and perfused through the left cardiac ventricle with 0.9% saline until the fluid from the right atrium was clear, followed by a brief (7–8 min) perfusion with 2% paraformaldehyde in 0.1 M phosphate buffer (pH 7.4). The brains were removed and photographed. Visual cortex was unfolded, flattened (Olavarria & Van Sluyters, 1985), and cut in the tangential plane (50 μ m in thickness) in a freezing microtome. Flattening a curved surface with little or no distortion requires making cuts at selected places along the border, much like cartographers do to create flat maps of the world (e.g., the Goode homolosine projection). We performed cuts at selected places of the galago cerebral cortex. The asterisk in Fig. 1C shows one of these cuts.

Histological procedures

The first 4–5 cortical tangential sections through the visual cortex were reacted for CO histochemistry according to the protocol in (Wong-Riley, 1979). The remaining tangential sections were reacted for HRP histochemistry with tetramethyl benzidine as the chromogen (Mesulam, 1978).

Data acquisition and analysis

The main aim of our study was the reconstruction of the pattern of ODCs in greater galago as completely as possible. To this end, we planned the CO and WGA-HRP staining protocol based on previous studies of the laminar organization of CO staining in galagos. Condo and Casagrande (1990) studied greater and lesser galagos and report that CO blobs are not observed in all layers. The darkest and most distinct CO blobs are observed in layers III. CO blobs are

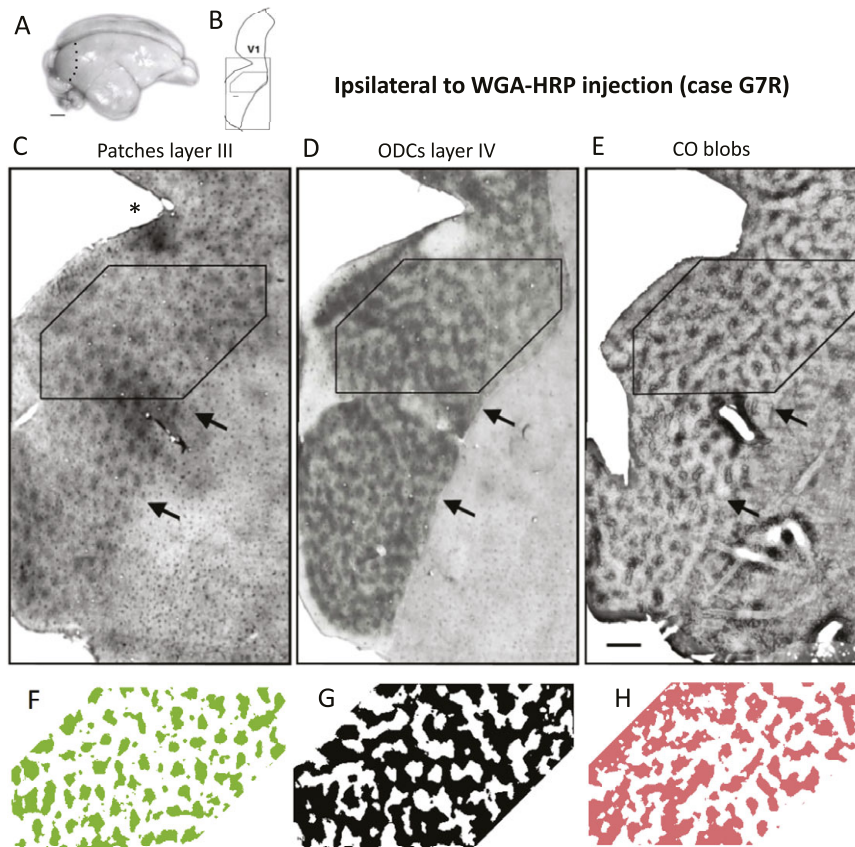


Fig. 1. WGA-HRP labeling in layers III and IV ipsilateral to the intraocular injection of WGA-HRP, and CO blobs in supragranular layers in Galago V1. (A) Galago brain showing the location of V1 in the occipital cortex of the right hemisphere. Dotted line indicates the anterior border of V1. (B) The rectangle indicates the region of the unfolded and flattened V1 shown in Fig. 1C–1E, and the box inside the rectangle outlines the common region analyzed in these images. (C,D) Labeling pattern in layers III and IV, respectively. (E) Pattern of CO blobs in the same hemisphere. Asterisk in C indicates cut at the edge of the cortical mantle during the flattening process. Arrows in C–E indicate the anterior border of V1. (F–H) Thresholded colored versions of the patterns in C–E, respectively. Scale bar in E = 1.0 mm.

also evident in upper layer IV ($IV\alpha$), but not in lower layer IV ($IV\beta$), where CO labeling is homogeneous throughout the layer. In layer V, large darkly CO-stained pyramidal cells are scattered throughout the layer without evidence of CO periodicity, and faint CO blobs are apparent in upper layer VI. The remainder of layer VI is uniformly and lightly stained. Condo and Casagrande (1990) also indicate that CO blobs in upper layer IV and layer VI are aligned with CO blobs in layer III.

Based on the above information, we did not alternate sections stained for CO and WGA-HRP because sections through layers that do not show clear CO periodicity would not yield useful CO data, but instead prevent these sections from being stained for WGA-HRP. A reduction in the number of WGA-HRP sections would most likely result in gaps in the reconstructed patterns of ODCs.

Individual tangential sections containing CO or WGA-HRP labeling were scanned (Epson 4990), and the resulting digital images were used to reconstruct the patterns of CO and HRP labeling in the primary visual cortex. The data were analyzed using Photoshop CS5 (Adobe Systems, San Jose, CA), and all image processing used, including contrast enhancement and intensity level adjustments, were applied to the entire images and never locally. Patterns of ODCs or CO over large areas were reconstructed by superimposing two or more sections in Photoshop. Unfolding and flattening the cortex facilitated the accurate alignment of tangential sections stained for CO or WGA-HRP

using radial blood vessels, tissue borders and other fiducial marks (Olavarria & Van Sluyters, 1985). Images in separate Photoshop layers were carefully aligned with each other and the final pattern of ODCs or CO were obtained by merging all images together. To facilitate obtaining thresholded images of the final ODC and CO patterns, images were high-pass filtered to remove gradual changes in staining density. The arrays of blood vessels in the WGA-HRP stained section were chosen for aligning the CO-stained sections typically show additional blood vessels that are not as visible in the sections stained for WGA-HRP. We did not correlate the patterns of WGA-HRP staining in layer VI with CO blobs.

To calculate the density and size of CO blobs, labeled patches in layers III and VI, thresholded images of these elements were analyzed using ImageJ. To calculate the density of a certain class of elements, we counted the number of elements in the sampled region, and then divided the number obtained by the total area of the sampled region. To measure the average size of a certain class of elements, we measured the total area occupied by a number of elements in each element class, and divided it by the number of elements in the sampled area (Table 1). Chi-square tests ($df = 1$, significance set at $P < 0.05$) were used to test whether labeled patches in layer III are aligned with ODCs of the same eye dominance in layer IV, and to analyze the distribution of CO staining over ipsilateral and contralateral ODCs.

Table 1. Coverage, size, and density of layer III patches, CO blobs, and layer VI patches

	% of area sampled in V1	Size (mm ²)	Number/mm ²	Total number in sample
Layer III patches	36.34	0.101	3.58	92
CO blobs	46.38	0.133	3.46	54
Layer VI patches	41.08	0.137	2.99	35

Results

To investigate the distribution of retino-geniculo-cortical input to striate cortex (V1) in greater galago, we injected the transneuronal tracer WGA-HRP into one eye and analyzed the patterns of WGA labeling in tangential sections through supragranular, granular, and infragranular layers of V1 in both hemispheres. The transneuronal anterogradely transport properties of WGA-HRP have been demonstrated at both the optical and structural level (Itaya & van Hoesen, 1982; Itaya et al., 1984). These properties ensure that the cortical labeling in these cortical targets corresponds to direct LGN projections (Itaya et al., 1984). In addition, we correlated the WGA-HRP labeling patterns with the distribution of CO blobs revealed in a separate set of tangential sections (Condo & Casagrande, 1990). We identified the cortical layers displaying WGA-HRP labeling by comparing our results with previous descriptions of retino-geniculate-cortical projections in galago revealed in parasagittal or coronal histological sections (Glendenning et al.,

1976; Casagrande & DeBruyn, 1982), or in tangential sections through V1 (Lachica & Casagrande, 1992). We describe the projection patterns in supragranular layer (layer III), granular layer (layer IV), and infragranular layer (layer VI), the correlation between WGA-HRP labeling patterns in layers III and IV, and the correlation of CO blobs with labeling patterns in layers III and IV.

The location of the area of galago V1 that is visible on the surface of the occipital lobe is indicated by the dotted line in Fig. 1A. V1 extends ventrally over the tentorium and medially on the dorsal and ventral banks of the calcarine fissure (Rosa et al., 1997). Unfolding and flattening the entire V1 required cutting along the fundus of the calcarine fissure (Fig. 1B). The rectangle in Fig. 1B indicates the region of V1 shown in Fig. 1C–1E, and the box inside the rectangle outlines the common region analyzed in these images. The asterisk in Fig. 1C indicates a cut made during the flattening procedure. Fig. 1C and 1D shows the labeling pattern in layers III and IV, respectively, in V1 ipsilateral to the WGA-HRP eye injection in galago 7, and Fig. 1E shows the patterns of CO blobs in the same region. For each pattern, a thresholded version of the common region is shown in color below each image (Fig. 1F–1H). Fig. 2 shows the use of radial penetrating blood vessels for aligning WGA-HRP and CO-stained tangential sections in Photoshop in galago 7. It shows that the matching blood vessels were distributed over large portions of the analyzed areas in the three histological sections, providing evidence that the alignment of the three sections was good over the analyzed area. See the legend to Fig. 2 for additional details. A similar procedure was used to analyze the other cases in this study. The relationships between the WGA-HRP and CO patterns in this case are shown in Fig. 3.

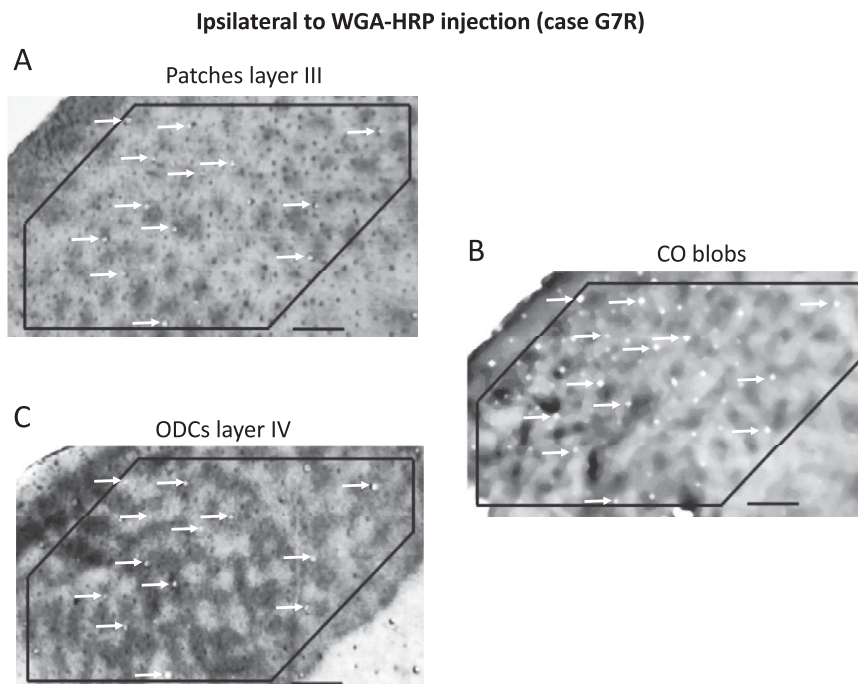


Fig. 2. Showing the use of radial penetrating blood vessels for aligning WGA-HRP and CO stained tangential sections in Photoshop. White arrows in A point to blood vessels that were judged to be present in the sections stained for WGA-HRP and CO in the case shown in Fig. 1 (galago 7). The set of arrows in A was displaced onto B (CO blobs) and onto C (ODCs) to point to the corresponding patterns of blood vessels in the three tangential sections. This figure shows that the matching blood vessels were distributed over large portions of the analyzed areas in the three histological sections, providing evidence that the alignment of the three sections was good over the analyzed area. See Materials and methods for additional details. Scale bar = 1 mm.

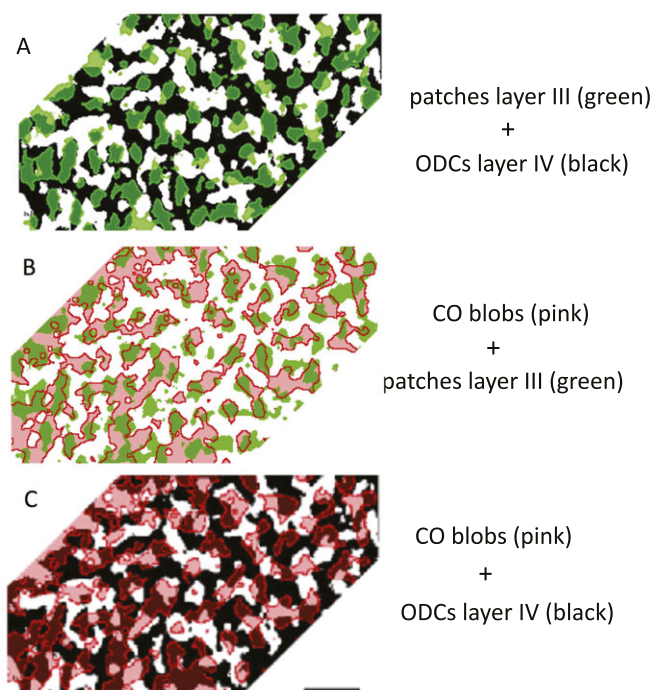


Fig. 3. Relationships between the WGA-HRP and CO labeling patterns in V1 ipsilateral to the eye injection in galago 7 shown in Fig. 1F–H. (A) Superimposition of the labeling pattern in layer III (green patches) over the pattern of ODCs in layer IV (black). (B) Superimposition of the pattern of CO blobs (pink) over the labeling pattern in layer III (green). (C) Superimposition of the pattern of CO blobs (pink) over the labeling of ODCs in layer IV (black). Scale bar = 1.0 mm.

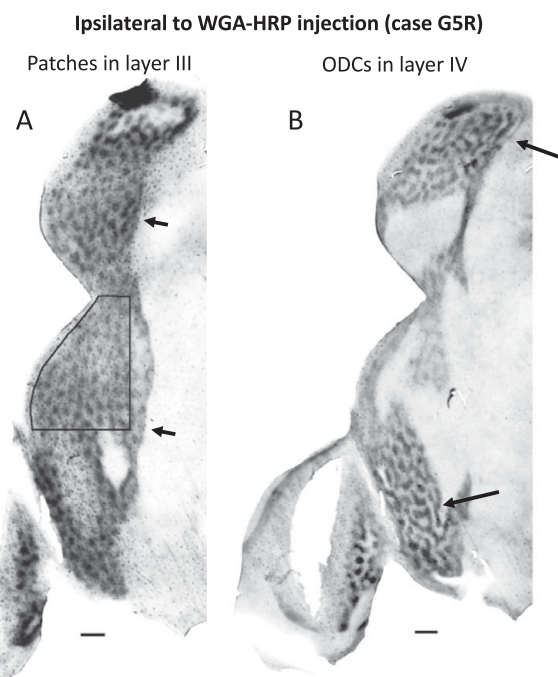


Fig. 4. Patterns of WGA-HRP labeling in layers III and IV in the hemisphere ipsilateral to the eye injection of WGA-HRP in galago 6. (A) Labeling in layer III. Arrows indicate the anterior border of V1. The box indicates region analyzed in Fig. 5. (B) Labeling pattern in layer IV in regions indicated by the arrows. Scale bar = 1.0 mm.

Retino-geniculo-cortical projections to layer III in V1

Projections to layer III were examined in hemispheres ipsilateral and contralateral to the WGA-HRP eye injection. In both hemispheres, WGA-HRP-labeled projections to layer III appear as arrays of distinct patches. Figs. 1C (galago 7) and 4A, 5A (galago 5) illustrate layer III projections. Patchy contralateral projections to layer III are shown in the section in Fig. 6A and 6B (galago 7), as well as in the immediately deeper section from the same case (Fig. 7A). Fig. 7A shows the patchy labeling pattern in layer III, except in the ventral region (white rectangle), which shows labeling in layer IV (described below). In this ventral region, it is interesting to notice that in both Figs. 6A and 7A, the labeling in the area marked with an asterisk is uniformly dense. This region represents the peripheral monocular segment innervated by the contralateral eye, as described in other primates (Horton & Hocking, 1996b), and the arrow next to the asterisk in Figs. 6A and 7A indicates the border of peripheral V1.

The labeled patches in layer III occupy 36.34% of the area analyzed in central V1. On average, they measure 0.101 mm² in area size, and the number of patches per unit area is 3.58 patches/mm². The patchy labeling in layer III most likely represents the patchy koniocellular input to layer III shown previously (Diamond et al., 1985; Lachica & Casagrande, 1992). Patchy labeling was not observed beyond the anterior border of V1, indicated by arrows in Figs. 1C and 4A.

Retino-geniculo-cortical projections to layer IV in V1

The distribution of projections to layer IV is strikingly different from that to layer III. Instead of isolated patches, the labeling in layer IV in both hemispheres forms patterns of interconnected bands or stripes 200–250 μm in width. Fig. 1D shows the labeling pattern in layer IV in the hemisphere ipsilateral to the eye injection in galago 7. A similar pattern in layer IV was observed in the hemisphere ipsilateral to the eye injection in galago 5 (long arrows in Fig. 4B), as well as in the hemisphere contralateral to the eye injection (Fig. 7B). Fig. 7B shows a magnified view of the area outlined by the white rectangle in Fig. 7A.

The pattern of ODCs we observed in galago layer IV resembles the pattern of ODCs in the cat layer IV (Anderson et al., 1988), squirrel monkey (Horton & Hocking, 1996a) and owl monkey (Takahata et al., 2014). Moreover, as in these species, the bands or stripes in galago layer IV do not appear to have a preferred orientation across V1, and, in particular, they do not tend to meet the border of V1 at right angles, as in macaque monkeys (Florence & Kaas, 1992; Horton & Hocking, 1996b; Fig. 6 in Olavarria & Van Essen, 1997). Ipsilateral labeled layer IV ODCs occupy 60.59% of the area examined, while contralateral labeled layer IV ODCs occupy 58.88% of the area examined, suggesting some overlap between right and left ODCs in layer IV.

Relation between layer III patches and layer IV ODCs

Layer III patches in galago have been revealed after tracer injections into eye-specific K LGN layers (Lachica & Casagrande, 1992), following transneuronal transport of tracers after monocular tracer injections (Casagrande & DeBruyn, 1982), and patchy activation patterns have been revealed with imaging techniques following monocular stimulation in galago (Xu et al., 2005) and owl monkey (Kaskan et al., 2007). A question not addressed by previous studies is whether layer III patches are randomly distributed in V1, or

whether they are aligned with layer IV bands of the same eye dominance. Fig. 3A shows the superimposition of the pattern of layer III patches over the pattern of ODCs in layer 4 from the case in Figs. 1 and 2. Inspection of Fig. 3A suggests that layer III patches (green) are preferentially aligned with layer 4 ODCs (black). To address this issue quantitatively, we performed a χ^2 analysis of the distribution of labeling in layers III and IV in both hemispheres following an injection of WGA-HRP into one eye of galago 7. For a random distribution of layer III patches, the proportion of labeled layer III patches over labeled and unlabeled ODCs in layer IV should be equal to the proportion of areas covered by labeled and unlabeled ODCs, respectively. Our analysis showed that the proportion of ipsilateral labeled layer III patches over ipsilateral labeled layer 4 ODCs was greater than expected (74.58%; expected 60.59%), while the proportion of ipsilateral labeled layer III patches over unlabeled contralateral layer 4 ODCs was smaller than expected (25.42%; expected 39.40%), $\chi^2 = 8.19$, $df = 1$, $P < 0.01$. Similarly, the proportion of contralateral labeled layer III patches over contralateral labeled layer 4 ODC was greater than expected (70.758%; expected 58.887%), while the proportion of contralateral labeled layer III patches over unlabeled ipsilateral layer IV ODCs was smaller than expected (29.241%; expected 41.112%), $\chi^2 = 5.82$, $df = 1$, $P < 0.05$. These results reject the null hypothesis that labeled layer III patches are distributed randomly over V1, and suggest that the radial registration of eye-specific geniculocortical projections to different cortical layers is largely maintained even when the direct projections to these layers originate from different cells types in the LGN.

Retino-geniculo-cortical projections to layer VI in V1

It is known that in galagos, as in macaques, P and M geniculate cells send relatively minor projections to layer VI (reviewed in Casagrande & Kaas, 1994), but the overall pattern of these projections is not currently known. In the New World spider monkey, Florence et al. (1986) studied ocular segregation in striate cortex following intraocular injections of tritiated proline in one eye. They found that the projections to layer VI are considerably lighter than those to layer IV and do not show clear evidence of ocular periodicity. We found that retino-geniculate projections to galago layer VI form patches that are somewhat less distinct than the patches in layer III. Fig. 8A and 8B shows labeled patches in layer VI ipsilateral and contralateral to the WGA-HRP injection, respectively, in galago 7, anterior is to the right in both images. The labeled patches in layer VI occupy 41.08% of the area analyzed in central V1, and on average, they measure 0.137 mm² in area size, and the number of patches per unit area is 2.99 patches/mm². Compared with labeled patches in layer III, layer VI patches appear to be somewhat larger, cover a larger area of V1, and their number per unit area is smaller (Table 1). It will be interesting to determine whether layer VI patches segregate by eye dominance and whether they correlate with patches in layer III, ODCs in layer IV, and CO blobs in upper layer VI (Condo & Casagrande, 1990). In the cat, injections of tritiated proline into LGN layers (LeVay & Gilbert, 1976), or WGA-HRP injections into one eye (Olavarria, unpublished results) reveal columnar projection to layer VI that are in register with ODCs in layer IV.

Correlation between CO blobs and layer III WGA-HRP labeled patches

In macaque and squirrel monkeys, Livingstone and Hubel (1982) reported that injections of either tritiated proline or HRP into the

LGN revealed an array of patches that appeared to match the array of CO blobs in layer III, but it was not resolved whether this projection was direct, or indirect via layer IV. Similar results have been reported in owl monkey (Ding & Casagrande, 1997) and squirrel monkey (Fitzpatrick et al., 1983). In greater galago, Lachica & Casagrande, 1992 demonstrated that K LGN layers project directly to layer III, and that single axons labeled by injections of WGA-HRP or *Phaseolus vulgaris* leucoagglutinin (PHA-L) into K LGN layers arborize within CO blobs in layer III (Lachica & Casagrande, 1992). Our results confirm and extend these previous findings in galago by providing evidence that virtually all CO blobs in V1 receive K LGN input from both eyes.

Fig. 1E shows the distribution of CO blobs in the hemisphere ipsilateral to the WGA-HRP injection in galago 7, and Fig. 3B correlates the distribution of CO blobs (pink) with the distribution of WGA-HRP labeled patches in layer III (green). This figure shows that virtually all CO blobs overlap with WGA-HRP labeled patches in layer III. Results from the hemisphere ipsilateral to the eye injection in galago 5 are shown in Fig. 5. The pattern of layer III patches (Fig. 5A) and the pattern of CO blobs (Fig. 5B) are superimposed in Fig. 5C. Fig. 5C shows that virtually all CO blobs (grey) overlap with the patches of K LGN input in layer III (black). Similar results were observed in the hemispheres contralateral to the eye injection. Fig. 6A shows the distribution of contralateral WGA-HRP labeled patches in layer III in galago 7. The region analyzed is outlined in black and shown at higher magnification in Fig. 6B. Fig. 6C shows the pattern of CO blobs in the same region, and

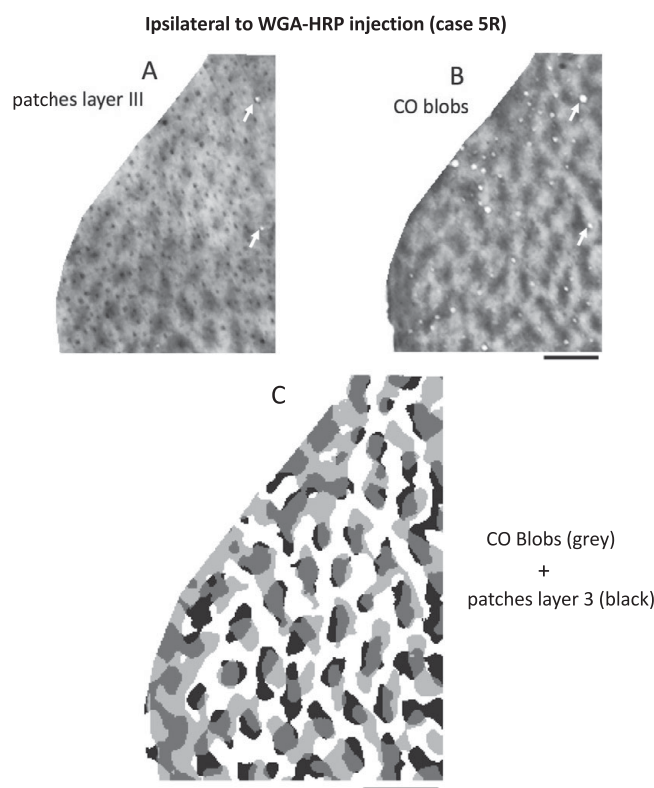


Fig. 5. Correlation between the WGA-HRP labeling pattern in layer III and the pattern of CO blobs in hemisphere ipsilateral to the eye injection in galago 5. The analyzed region is indicated by the box in Fig. 4. (A) Pattern of labeled patches in layer III. (B) Pattern of CO blobs. (C) Superimposition of CO blobs (grey) over labeled patches in layer III (black). White arrows in A, B indicate some of the blood vessels used to superimpose patterns in A and B. Scale bars in B, C = 1.0 mm.

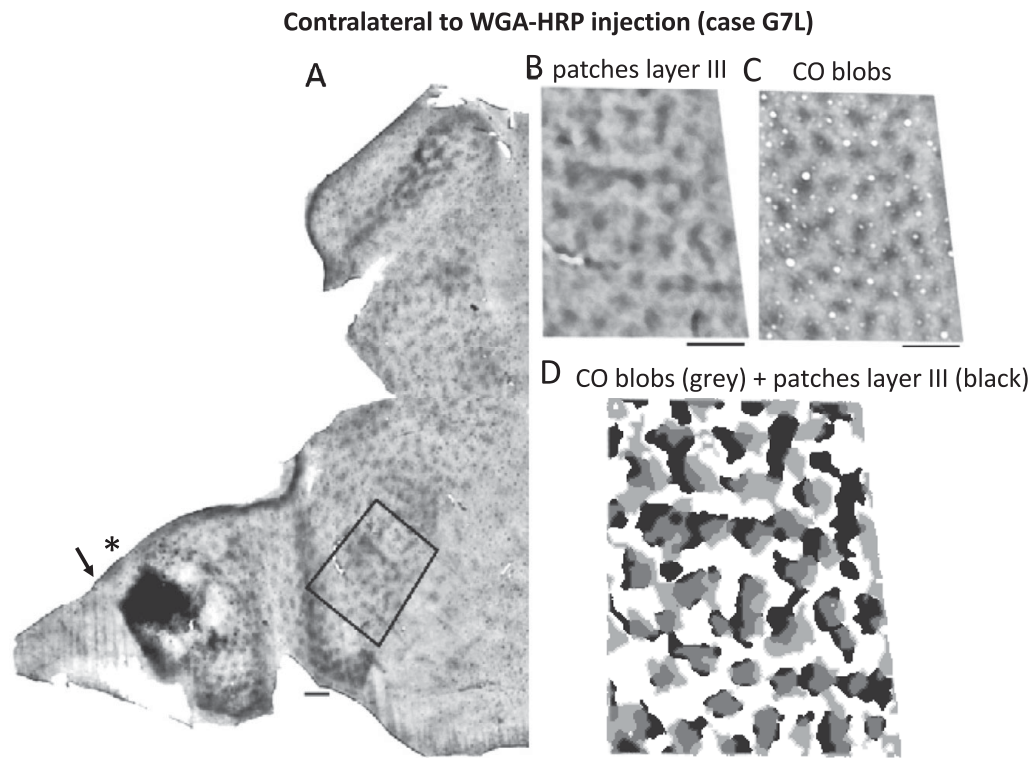


Fig. 6. Correlation between the WGA-HRP labeling pattern in layer III and the pattern of CO blobs in hemisphere contralateral to the eye injection in galago 7. **(A)** Overall pattern of labeling in layer III. The analyzed region is indicated by the box in **A**. **(B)** Pattern of labeled patches in layer III. **(C)** Pattern of CO blobs in the same region. **(D)** Thresholded patterns of CO blobs (grey) over labeled patches in layer III (black) are superimposed. Asterisk in **A** indicates region of homogeneous labeling in the peripheral monocular segment of V1, and the arrow indicated the peripheral border of V1. Scale bars in **A–D** = 1.0 mm.

Fig. 6D shows the correlation between the labeled layer III patches (black) and the pattern of CO blobs (grey) from the same region. Again, we observed that virtually all CO blobs (grey) overlap with layer III patches (black). Moreover, Figs. 3B, 5C, and 6D provide evidence that layer III patches typically overlap with only a portion of the CO blobs, and that in some instance they extend beyond the borders of CO blobs, into the interblob region. Together, the results from hemispheres ipsilateral (Fig. 3B and 5C) and contralateral (Fig. 6D) to the eye injection provide strong support to the idea that all CO blobs in greater galagos receive K LGN input from both eyes. We estimate that CO blobs occupy about 46.38% of the area analyzed in V1. On average, CO blobs measure 0.133 mm^2 in size, they occupy 46.38% if the area sampled in V1, and there are 3.46 blobs/mm^2 . Comparison of CO blobs with layer III labeled patches suggests that CO blobs occupy a larger area of V1 and are larger in size, but the number of CO blobs and layer III patches per unit area is very similar (Table 1).

Correlation between CO blobs and layer IV ODCs

Previous studies have shown that CO blobs are located at the center of ODCs in macaques (Horton, 1984; Blasdel & Salama, 1986; Tootell et al., 1988; Bartfeld & Grinvald, 1992; Yoshioka et al., 1996). With the exception of *Cebus apella* (capuchin) monkey (Hess & Edwards, 1987; Rosa et al., 1992), a clear and consistent correlation between CO blobs and ODCs has not been found in New World primates (Roe et al., 2005; Kaskan et al., 2007; Takahata et al., 2014). Similarly, an optical imaging study of intrinsic signals in galago observed no clear relationship between the distribution of CO blobs and the ocular dominance domains (Xu et al., 2005). We

found that individual CO blobs consistently straddle the border between neighboring ipsilateral and contralateral layer IV ODCs. Fig. 3C (galago 7, ipsilateral to the eye injection) shows the pattern of CO blobs (pink) superimposed on the pattern of ipsilateral (black) and contralateral (white) ODCs, such that virtually each CO blob samples both ipsilateral (black) and contralateral (white) territories. Similar results were obtained in the hemisphere contralateral to the eye injection (Fig. 7, galago 7). The region analyzed is outlined by the white rectangle in Fig. 7A. The labeling pattern in layer IV in this region is enlarged in Fig. 7B and 7C shows the pattern of CO blobs in the same region (white arrows indicate some common blood vessels). For each of these two patterns, a thresholded version of the common region is shown in black and pink below each image, and the relationship between these patterns is shown in Fig. 7D. As in Figs. 3C, 7D shows that virtually all CO blobs (pink) straddle the border between neighboring ODCs, such that each CO blob overlaps with labeled (black) and unlabeled (white) layer IV ODCs. The yellow square outlines the region displayed in Fig. 9 (see Discussion).

We also examined 3 hemispheres from two additional cases injected with WGA-HRP into one eye (galago 3 and galago 6), and the results confirm our observations from the cases described above regarding the distribution of layer-specific patterns of WGA-HRP labeling, and their correlation with CO blobs (data not shown).

Percentage of CO staining that overlaps with ipsilateral and contralateral ODCs

Our results showing that CO blobs are not centered on ODCs, but rather span the borders between ODCs raise the question about the

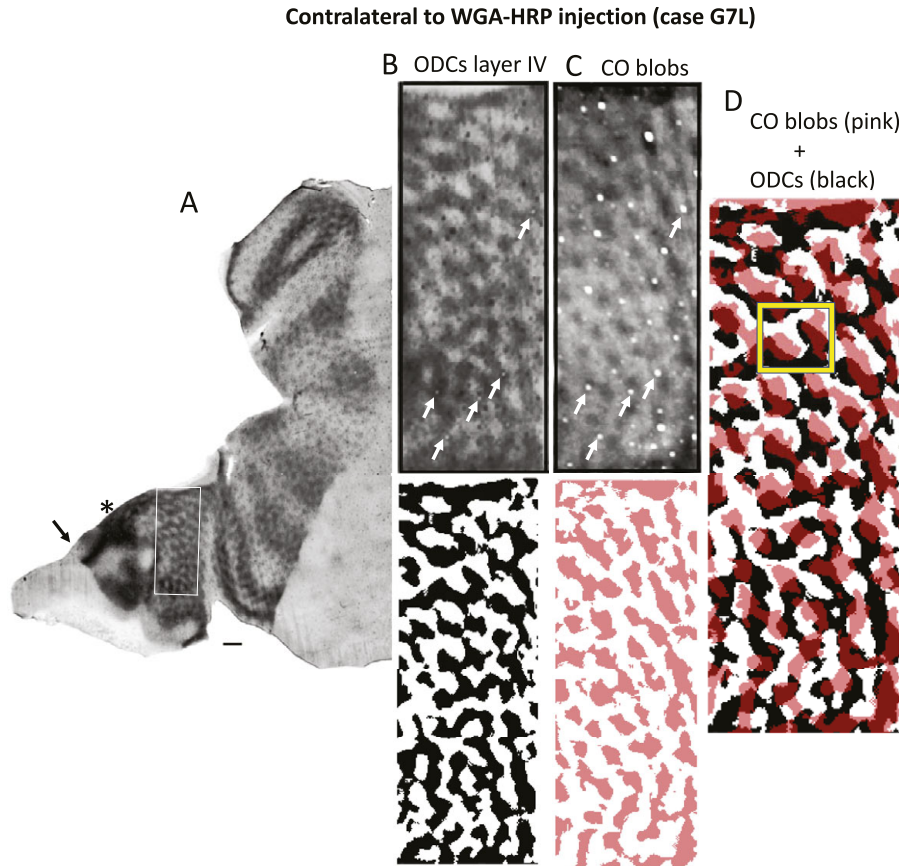


Fig. 7. Correlation between the WGA-HRP labeling pattern in layer IV and the pattern of CO blobs in hemisphere contralateral to the eye injection in galago 7. (A) Overall pattern of WGA-HRP labeling. The region outlined by the white box shows labeling in layer IV. This region is magnified in (B). (C) Pattern of CO blobs in the same region. White arrows in B, C indicate some of the blood vessels used to superimpose patterns in B and C. Corresponding thresholded patterns are shown below for ODCs in layer 4 (black) and CO blobs (pink). (D) Superimposition of CO blobs (pink) over contralateral (black) and ipsilateral (white) ocular dominance columns in layer IV. The yellow box outlines a region used in Fig. 9. Scale bars in A = 1.0 mm.

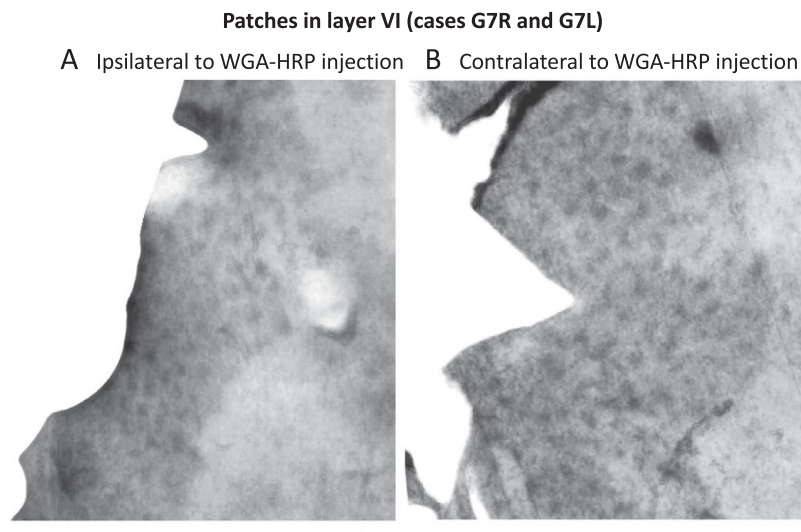


Fig. 8. Overall pattern of WGA-HRP labeling in layer VI in hemispheres ipsilateral (A) and contralateral (B) to the eye injection in galago 7. Scale bars = 1.0 mm.

fractional distribution of CO labeling over ipsilateral and contralateral ODCs in layer IV. We addressed this question by performing a chi-square analysis of the distribution of CO labeling over ipsilateral and contralateral ODCs in layer IV in both hemispheres

following an intraocular injection of WGA-HRP in galago 7 (Figs. 1 and 7). We tested the hypothesis that the distribution of CO labeling over ipsilateral and contralateral ODCs is non-biased. For a non-biased distribution, the proportion of CO labeling over

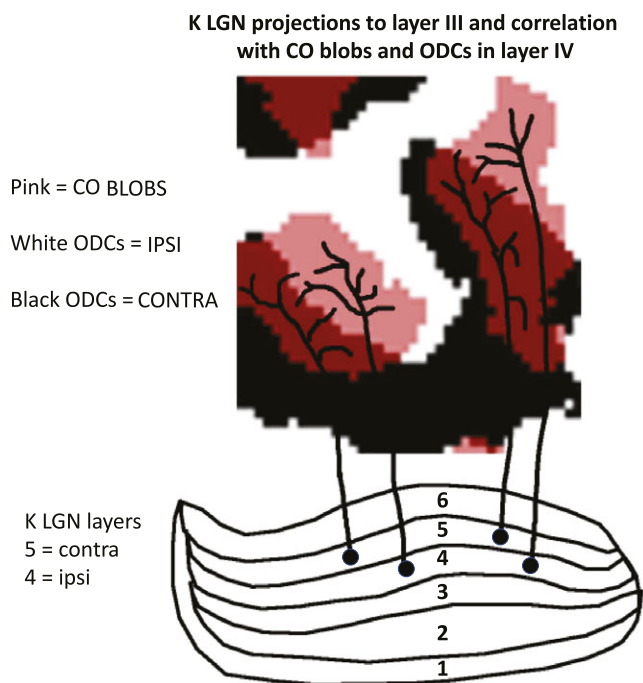


Fig. 9. Diagram based on the case shown in Fig. 7D (region outlined in yellow in Fig. 7D). It shows that individual CO blobs (pink) overlap with labeled (black) and unlabeled (white) ODCs in layer IV. It also shows that the sizes of the arborizations of afferents from ipsilateral and contralateral K LGN layers (represented as branching black lines) may be largely constrained by the sizes of the CO blob subregions of the same eye dominance. Cells in ipsilateral and contralateral K LGN layers (layers 4 and 5, respectively) are represented as black dots.

labeled and unlabeled ODCs in layer IV should be equal to the proportion of areas covered by labeled and unlabeled ODCs, respectively. Our analysis showed that the proportion of CO labeling over ipsilateral labeled layer 4 ODCs was 62% (expected 60.59%), while the proportion of CO labeling over contralateral unlabeled ODCs was 38% (expected 39.41%), $\chi^2 = 0.083$, $df = 1$, $P > 0.05$. Similarly, the proportion of CO labeling over contralateral labeled layer 4 ODCs was 54% (expected 58.88%), while the proportion of CO labeling over ipsilateral unlabeled ODCs was 46% (expected 41.12%), $\chi^2 = 0.985$, $df = 1$, $P > 0.05$. These results do not reject the tested hypothesis, suggesting that, although not centered on ODCs, CO blobs in galago sample ipsilateral and contralateral ODCs in a non-biased manner.

Discussion

Overall pattern of layer IV ocular dominance columns in greater galago V1

We revealed, for the first time, that ODCs in greater galago layer 4 form a relatively continuous system of irregularly branching bands, about 200–250 μm in width, in the hemispheres contralateral and ipsilateral to the injected eye. This pattern resembles the patterns of ODCs in cat layer IV (Anderson et al., 1988; Olavarria, 2001), squirrel monkey (Horton & Hocking, 1996a), and owl monkey (Takahata et al., 2014). Moreover, as in these species, the bands in galago layer IV do not appear to have a bias in the distribution of orientations, and do not meet the border of V1 at right angles. In contrast, in macaque (e.g., Fig. 6 in Olavarria & Van Essen, 1997), and the New World monkey *C. apella* (Rosa et al.,

1992), ODCs appear as largely parallel stripes that intersect the V1 border at approximately right angles. One factor that may influence the orientation of ODCs is the emphasis on central visual representation in V1. Rosa et al. (1997) report that, in galago, the emphasis on central visual field representation in V1 is significantly less than in other primate species, but comparable to that of other non-primates, like cats. Another factor considered in previous studies is the overall shape of V1, and how the contralateral and ipsilateral visual fields are represented with respect to the main axes of V1. Anderson et al. (1988) point out that while the shape of V1 is elliptical in both macaque and cat, such that the ratio between long and short axes is nearly identical in both species, the horizontal meridian runs along the long axis of V1 in macaques, while in cats it runs along the short axis. This 90-deg rotation of the visual hemifield map in V1 would impose different constraints for accommodating the alternate mapping of contralateral and ipsilateral slices of the visual field, resulting in the pattern observed in the cat, in which the contralateral and ipsilateral strips alternate forming seemingly random patterns (Anderson et al., 1988; Olavarria, 2001). Interestingly, in rats, as in cats, V1 is elliptical in shape and the horizontal meridian runs along the short axis of V1. ODCs in this rodent form patches of various shapes and sizes that show no orientation bias with respect to the V1 border (Laing et al., 2015; Olavarria et al., 2021). In galago (Rosa et al., 1997) and squirrel monkey (Horton & Hocking, 1996a), V1 is nearly circular in shape, which could impose constraints leading to the development of irregularly branching eye-specific bands. More recently, Najafian et al. (2019) proposed a cortical model that generates variations in ocular dominance patterns from variations in local cortical retinotopy. They describe a common organizing principle across species that aligns the cortical axis of ocular dominance segregation with the axis of the slowest retinotopic gradient, arguably accounting for ODCs patterns as diverse as those in macaques, squirrel monkey, cats and rats.

CO blobs in galago V1 straddle the border of ocular dominance columns and receive largely segregated K LGN projections from both eyes

Lachica and Casagrande (1992) injected the K LGN layers in galago with anterograde tracers and reported that terminations from individual K LGN axons form arbors of different sizes that are restricted to CO blobs, typically arborizing in only a fraction of the target CO blob. Our approach gave us the opportunity to examine the relationship between layer III patches and CO blobs in broad regions of both ipsilateral and contralateral hemispheres in the same animal. In each hemisphere, we found that virtually all CO blobs overlap with patches of K LGN projections in layer III. The overlap between layer III patches and CO blobs is partial, indicating that layer III patches occupy only a portion of the CO blob, in agreement with Lachica and Casagrande (1992). Our results imply that virtually all CO blobs receive K LGN input from both eyes. In addition, our data show that in some instances, the K LGN input extends into the neighboring interblob region. This observation would seem to be at odds with the report by Lachica and Casagrande (1992) that terminations of individual axons are restricted to CO blobs. We believe that the study by these authors does not necessarily contradict our results because we did observe many instances in which the layer III projections were largely or entirely restricted to the CO blobs. Moreover, Ding and Casagrande (1997) reported that, in owl monkeys, “the K terminals appear, in most cases, to extend slightly beyond the blob borders”. Lachica and

Casagrande (1992) reconstructed a small sample of axons from parasagittal sections, and is possible that, by chance, the axon terminations they reconstructed were restricted to CO blobs. The function of K projections to CO blobs is discussed in Lachica et al. (1992) and Ding and Casagrande (1997), but, at present, the possible function of K LGN projections to interblob regions in layer III remains to be investigated.

We also documented that CO blobs consistently straddle the border between neighboring ipsilateral and contralateral ODCs in layer IV, such that the percentage distribution of CO staining over ipsilateral and contralateral ODCs is approximately equal. Moreover, a chi-square analysis showed that layer III patches are significantly correlated with layer IV ODCs of the same eye dominance. Together, our findings suggest that K LGN projections from each eye are largely segregated into ipsilateral and contralateral territories within the CO blobs. Support for this idea comes from previous physiological studies reporting that a high percentage of cells in CO blobs in galago V1 are monocular (DeBruyn et al., 1993). This idea is also consistent with our estimate that the average size of CO blobs is larger than the average size of layer III patches, while the average number of CO blobs per unit area is very similar to the average number of layer III patches labeled following an injection of WGA-HRP into one eye (Table 1). Fig. 9, based on the case shown in Fig. 7D (region outlined in red in Fig. 7D), shows and summarizes these findings. It depicts that individual CO blobs (pink) overlap with labeled (black) and unlabeled (white) ODCs in layer 4. Fig. 9 also proposes that the sizes of the arborizations of afferents from ipsilateral and contralateral K LGN layers (represented as branching black lines) are largely constrained by the sizes of the CO blob subregions of the same eye dominance. Our finding that CO blobs consistently straddle the border between ODCs contrasts with the results of an optical imaging study of intrinsic signals in galago, which found no clear relationship between the distribution of CO blobs and the ocular dominance domains (Xu et al., 2005). The different outcomes may be attributed to differences in the methodology used in both studies.

In Old World macaque monkeys (Horton, 1984; Blasdel & Salama, 1986; Tootell et al., 1988; Bartfeld & Grinvald, 1992; Yoshioka et al., 1996), New World Cebus monkeys (Hess & Edwards, 1987; Rosa et al., 1992), and humans (Adams et al., 2007), CO blobs are centered on ODCs and appear to be dominated by the monocular input represented in the underlying ODC (Livingstone & Hubel, 1984). The model we propose in galago (Fig. 9) can be hypothetically transformed into a model isomorphic with the macaque model by dividing the galago CO blobs into their two eye dominance regions, and then displacing each region toward the center of the underlying ODC of the same eye dominance. It would be interesting to determine whether there is a phylogenetic relation between the models for galago and macaque monkey. However, the fact that a clear and consistent correlation between CO blobs and ODCs has not been found in some New World primates (Roe et al., 2005; Kaskan et al., 2007; Takahata et al., 2014) suggests that other structural and functional relationships between CO blobs and ODCs may operate in these primates. In owl monkey, Takahata et al. (2014) found that ODCs adopt the form of interconnected bands or stripes, whereas they tend to be patchy in peripheral regions of V1. Moreover, these authors found that CO blobs straddle the border of ODCs in central regions of V1, but they are centered on ODCs patches in peripheral V1. The possibility that differences in the balance of left and right eye dominance in central *versus* peripheral regions of V1 influence

the correlation between CO blobs and ODCs is discussed in Takahata et al. (2014).

Our finding in greater galago that ODCs are irregular and CO blobs straddle the border of ODCs differs from the arrangement of ODCs and CO blobs in primate species that have larger brains, such as New World Cebus monkey and Old World macaque monkey (see Refs. above). It is possible that different arrangements of CO blobs with respect to ODCs may result from the application of similar developmental rules to brains of different sizes, depending on factors such as the area size and shape of V1. If so, differences among New World and Old World species may reflect developmental factors such as competition for cortical space in brains of different sizes, rather than differences across taxonomic boundaries.

Finally, it has been reported that monocular enucleation in young New World (Rosa et al., 1991) and Old World (Horton & Hocking, 1998) monkeys induces a reduction in the size of CO blobs centered on deprived ODCs, and an increase in the size of CO blobs centered on non-deprived ODCs. It would be interesting to study the effect of monocular enucleation or deprivation in greater galagos, given that CO blobs would typically straddle both deprived and non-deprived ODCs.

Comparison with cats

Previous studies have shown that parallel visual processing streams (Leventhal et al., 1985; reviewed in Casagrande & Norton, 1991) and CO blobs in V1 (Murphy et al., 1995; Boyd & Matsubara, 1996) exist in cats. As in primates, parallel retino-cortical pathways in cats originate from three distinct classes retinal ganglion cells, named X, Y, and W, which, on the basis of their appearance and physiological properties, have been compared to P, M, and K ganglion cells in primates, respectively (Leventhal et al., 1985; reviewed in Casagrande & Norton, 1991). Boyd and Matsubara (1996) report that projections from W cells (K-like) in cat LGN layers C1 and C2 are patchy in layer III of V1, and that the patches align with CO blobs, resembling the projection from K LGN layers to CO blobs described in galago (Lachica & Casagrande, 1992; Casagrande & Kaas, 1994; present study). It remains to be investigated whether all CO blobs in cat V1 receive W LGN projections from both eyes, as we found in this study to be the case for K LGN projections in galago. Regarding the position of CO blobs with respect to ODCs in cat layer IV in V1, Murphy et al. (1995) reported that the location of some CO blobs in V1 is not above the center of labeled ODCs. However, after considering that, relative to the width of ODCs, the diameter of CO blobs in cats is greater than in macaques, and that in cats there is some overlap between ipsilateral and contralateral ODCs, these authors proposed that the functional organization of the blobs is similar in cats and macaque monkeys. Galagos also resemble cats in the distribution of callosal connection in V1. In galagos (Weyand & Swadlow, 1980; Cusick et al., 1984; Beck & Kaas, 1994), as in cats (Boyd & Matsubara, 1994; Olavarria, 2001), callosal connections in V1 are robust and occupy a broad area extending medially from the V1/V2 border. In cats, callosal cells correlate with contralateral ODCs within the narrow V1/V2 transition zone (TZ), and with ipsilateral ODCs in regions of areas V1 and V2 located outside the TZ. Finding that ODCs in galago show the same association with visual callosal connections would suggest that the retinally driven mechanism that is thought to specify the distribution of callosal connections in cat V1 (Olavarria, 2001) also operates in galago.

In conclusion, our study is significant for mainly two reasons. It incorporates the greater galago into the group of primate and

non-primate species that have well-defined pattern of ODCs in layer IV of V1. In addition, our results suggest that ocular dominance is a key factor orchestrating the consistent relationship that we observed between ODCs in layer IV, CO blobs, and K LGN projections to CO blobs from both eyes (Fig. 9). Our findings in greater galago should facilitate, and serve as a reference for, future studies of the development, plasticity and function of ocular dominance domains and parallel visual pathways in Strepsirrhini primates.

Acknowledgments. We greatly acknowledge the guidance and help by Dr. Casagrande, and the technical support by personnel in the labs of Dr. Casagrande and Dr. Kaas. This research was supported by National Institutes of Health grant numbers: EY01778, EY02686, EY09343 (to J.H.K.), EY016045, NS070022 (to J.F.O.), and by National Natural Science Foundation of P. R. China 32170992, 31872767 (to T.T.).

Competing interests. The authors have no competing interest to declare.

References

- Adams, D.L., Sincich, L.C. & Horton, J.C. (2007). Complete pattern of ocular dominance columns in human primary visual cortex. *The Journal of Neuroscience* **27**, 10391–10403.
- Anderson, P.A., Olavarria, J. & Van Sluyters, R.C. (1988). The overall pattern of ocular dominance bands in cat visual cortex. *The Journal of Neuroscience* **8**, 2183–2200.
- Bartfeld, E. & Grinvald, A. (1992). Relationships between orientation-preference pinwheels, cytochrome oxidase blobs, and ocular-dominance columns in primate striate cortex. *The Proceedings of the National Academy of Sciences* **89**, 11905–11909.
- Beck, P.D. & Kaas, J.H. (1994). Interhemispheric connections in neonatal owl monkeys (*Aotus trivirgatus*) and galagos (*Galago crassicaudatus*). *Brain Research* **651**, 57–75.
- Blasdel, G.G. & Salama, G. (1986). Voltage-sensitive dyes reveal a modular organization in monkey striate cortex. *Nature* **321**, 579–585.
- Boyd, J. & Matsubara, J. (1994). Tangential organization of callosal connectivity in the cat's visual cortex. *The Journal of Comparative Neurology* **347**, 197–210.
- Boyd, J.D. & Matsubara, J.A. (1996). Laminar and columnar patterns of geniculocortical projections in the cat: Relationship to cytochrome oxidase. *The Journal of Comparative Neurology* **365**, 659–682.
- Casagrande, V.A. & DeBruyn, E.J. (1982). The galago visual system: Aspects of normal organization and developmental plasticity. In *The Lesser Bushbaby (Galago) as an Animal Model: Selected Topics*, ed. Haines, D.E., pp. 137–168. Boca Raton, FL: CRC Press.
- Casagrande, V.A. & Kaas, J.H. (1994). The afferent, intrinsic, and efferent connections of primary visual cortex in primates. In *Cerebral Cortex*, Vol. **10** (Chapter 5), ed. Peters, A. & Rockland, K.S., pp. 201–225. New York, NY: Plenum Press.
- Casagrande, V.A. & Norton, T.T. (1991). Lateral geniculate nucleus: A review of its physiology and function. In *The Neural Basis of Visual Function*, ed. Leventhal, A.G., pp. 41–84. New York, NY: Macmillan Press.
- Condo, G.J. & Casagrande, V.A. (1990). Organization of cytochrome oxidase staining in the visual cortex of nocturnal primates (*Galago crassicaudatus* and *Galago senegalensis*): I. Adult patterns. *The Journal of Comparative Neurology* **293**, 632–645.
- Cusick, C.G., Gould, H.J. & Kaas, J.H. (1984). Interhemispheric connections of visual cortex of owl monkeys (*Aotus trivirgatus*), marmosets (*Callithrix jacchus*), and galago (*Galago crassicaudatus*). *The Journal of Comparative Neurology* **230**, 311–336.
- DeBruyn, E.J., Casagrande, V.A., Beck, P.D. & Bonds, A.B. (1993). Visual resolution and sensitivity of single cells in the primary visual cortex (V1) of a nocturnal primate (bush baby): Correlations with cortical layers and cytochrome oxidase patterns. *Journal of Neurophysiology* **69**, 3–18.
- Diamond, I.T., Conley, M., Itoh, K. & Fitzpatrick, D. (1985). Laminar organization of geniculocortical projections in *Galago senegalensis* and *Aotus trivirgatus*. *The Journal of Comparative Neurology* **242**, 584–610.
- Ding, Y. & Casagrande, V.A. (1997). The distribution and morphology of LGN K pathway axons within the layers and CO blobs of owl monkey V1. *Visual Neuroscience* **14**, 691–704.
- Fitzpatrick, D., Itoh, K. & Diamond, I.T. (1983). The laminar organization of the lateral geniculate body and the striate cortex in the squirrel monkey (*Saimiri sciureus*). *The Journal of Neuroscience* **3**, 673–702.
- Florence, S.L., Conley, M. & Casagrande, V.A. (1986). Ocular dominance columns and retinal projections in New World spider monkeys (*Ateles ater*). *The Journal of Comparative Neurology* **243**, 234–248.
- Florence, S.L. & Kaas, J.H. (1992). Ocular dominance columns in area 17 of Old World macaque and talapoin monkeys: Complete reconstructions and quantitative analyses. *Visual Neuroscience* **8**, 449–462.
- Glendenning, K.K., Kofron, E.A. & Diamond, I.T. (1976). Laminar organization of projections of the lateral geniculate nucleus to the striate cortex in Galago. *Brain Research* **105**, 538–546.
- Hess, D.T. & Edwards, M.A. (1987). Anatomical demonstration of ocular segregation in the retinogeniculocortical pathway of the New World capuchin monkey (*Cebus apella*). *The Journal of Comparative Neurology* **264**, 584–610.
- Horton, J.C. (1984). Cytochrome oxidase patches: A new cytoarchitectonic feature of monkey visual cortex. *Philosophical Transactions of the Royal Society B* **304**, 199–253.
- Horton, J.C. & Hocking, D.R. (1996a). Anatomical demonstration of ocular dominance columns in striate cortex of the squirrel monkey. *The Journal of Neuroscience* **16**, 5510–5522.
- Horton, J.C. & Hocking, D.R. (1996b). Intrinsic variability of ocular dominance column periodicity in normal macaque monkeys. *The Journal of Neuroscience* **16**, 7228–7339.
- Horton, J.C. & Hocking, D.R. (1998). Effect of early monocular enucleation upon ocular dominance columns and cytochrome oxidase activity in monkey and human visual cortex. *Visual Neuroscience* **15**, 289–303.
- Itaya, S.K., Itaya, P.W. & Van Hoesen, G.W. (1984). Intracortical termination of the retino-geniculo-striate pathway studied with transsynaptic tracer (wheat germ agglutinin-horseradish peroxidase) and cytochrome oxidase staining in the macaque monkey. *Brain Research* **304**, 303–310.
- Itaya, S.K. & van Hoesen, G.W. (1982). WGA-HRP as a transneuronal marker in the visual pathways of monkey and rat. *Brain Research* **236**, 199–204.
- Kaskan, P.M., Lu, H.D., Dillenburger, B.C., Roe, A.W. & Kaas, J.H. (2007). Intrinsic-signal optical imaging reveals cryptic ocular dominance columns in primary visual cortex of New World owl monkeys. *Frontiers in Neuroscience* **1**, 67–75.
- Lachica, E.A., Beck, P.D. & Casagrande, V.A. (1992). Parallel pathways in macaque monkey striate cortex: Anatomically defined columns in layer III. *The Proceedings of the National Academy of Sciences* **89**, 3566–3570.
- Lachica, E.A. & Casagrande, V.A. (1992). Direct W-like geniculate projections to the cytochrome oxidase (CO) blobs in primate visual cortex: Axon morphology. *The Journal of Comparative Neurology* **319**, 141–158.
- Laing, R.J., Turecek, J., Takahata, T. & Olavarria, J.F. (2015). Identification of eye-specific domains and their relation to callosal connections in primary visual cortex of long Evans rats. *Cerebral Cortex* **25**, 3314–3329.
- LeVay, S. & Gilbert, C.D. (1976). Laminar patterns of geniculocortical projection in the cat. *Brain Research* **113**, 1–19.
- Leventhal, A.G., Rodieck, R.W. & Dreher, B. (1985). Central projections of cat retinal ganglion cells. *The Journal of Comparative Neurology* **237**, 216–226.
- Livingstone, M.S. & Hubel, D.H. (1982). Thalamic inputs to cytochrome oxidase-rich regions in monkey visual cortex. *The Proceedings of the National Academy of Sciences* **79**, 6098–6101.
- Livingstone, M.S. & Hubel, D.H. (1984). Anatomy and physiology of a color system in the primate visual cortex. *The Journal of Neuroscience* **4**, 309–356.
- Mesulam, M.M. (1978). Tetramethyl benzidine for horseradish peroxidase neurohistochemistry: A non-carcinogenic blue reaction product with superior sensitivity for visualizing neural afferents and efferents. *Journal of Histochemistry and Cytochemistry* **26**, 106–117.

- Murphy, K.M., Jones, D.G. & Van Sluyters, R.C. (1995). Cytochrome-oxidase blobs in cat primary visual cortex. *The Journal of Neuroscience* **15**, 4196–4208.
- Najafian, S., Jin, J. & Alonso, J.M. (2019). Diversity of ocular dominance patterns in visual cortex originates from variations in local cortical retinotopy. *The Journal of Neuroscience* **39**, 9145–9163.
- Olavarria, J.F. (2001). Callosal connections correlate preferentially with ipsilateral cortical domains in cat areas 17 and 18, and with contralateral domains in the 17/18 transition zone. *The Journal of Comparative Neurology* **433**, 441–457.
- Olavarria, J.F., Laing, R.J. & Andelin, A.K. (2021). Ocular dominance columns in V1 are more susceptible than associated callosal patches to imbalance of eye input during precritical and critical periods. *The Journal of Comparative Neurology* **529**, 2883–2910.
- Olavarria, J.F. & Van Essen, D.C. (1997). The global pattern of cytochrome oxidase stripes in visual area V2 of the macaque monkey. *Cerebral Cortex* **7**, 395–404.
- Olavarria, J. & Van Sluyters, R.C. (1985). Unfolding and flattening the cortex of gyrencephalic brains. *Journal of Neuroscience Methods* **15**, 191–202.
- Roe, A.W., Fritsches, K. & Pettigrew, J.D. (2005). Optical imaging of functional organization of V1 and V2 in marmoset visual cortex. *The Anatomical Record Part A Discoveries in Molecular Cellular and Evolutionary Biology* **287**, 1213–1225.
- Rosa, M.G.P., Casagrande, V.A., Preuss, T. & Kaas, J.H. (1997). Visual field representation in striate and prestriate cortices of a prosimian primate (*Galago garnetti*). *Journal of Neurophysiology* **77**, 3193–3217.
- Rosa, M.G.P., Gattass, R., Fiorani, M. Jr. & Soares, J.G.M. (1992). Laminar, columnar and topographic aspects of ocular dominance in the primary visual cortex of Cebus monkeys experimental. *Brain Research* **88**, 249–264.
- Rosa, M.G.P., Gattass, R. & Soares, J.G.M. (1991). A quantitative analysis of cytochrome oxidase-rich patches in the primary visual cortex of Cebus monkeys: Topographic distribution and effects of late monocular enucleation. *Experimental Brain Research* **84**, 195–209.
- Takahata, T., Miyashita, M., Tanaka, S. & Kaas, J.H. (2014). Identification of ocular dominance domains in New World owl monkeys by immediate-early gene expression. *The Proceedings of the National Academy of Sciences* **111**, 4297–4302.
- Tootell, R.B., Hamilton, S.L., Silverman, M.S. & Switkes, E. (1988). Functional anatomy of macaque striate cortex. I. Ocular dominance, binocular interactions, and baseline conditions. *The Journal of Neuroscience* **8**, 1500–1530.
- Weyand, T.G. & Swadlow, H.A. (1980). Interhemispheric striate projections in the prosimian primate, *Galago senegalensis*. *Brain Behavior and Evolution* **17**, 473–477.
- Wong-Riley, M. (1979). Changes in the visual system of monocularly sutured or enucleated cats demonstrable with cytochrome oxidase histochemistry. *Brain Research* **171**, 11–28.
- Xu, X., Bosking, W.H., White, L.E., Fitzpatrick, D. & Casagrande, V.A. (2005). Functional organization of visual cortex in the prosimian bush baby revealed by optical imaging of intrinsic signals. *Journal of Neurophysiology* **94**, 2748–2762.
- Yoshioka, T., Blasdel, G.G., Levitt, J.B. & Lund, J.S. (1996). Relation between patterns of intrinsic lateral connectivity, ocular dominance, and cytochrome oxidase-reactive regions in macaque monkey striate cortex. *Cerebral Cortex* **6**, 297–310.